THE JOURNAL OF PHYSICAL CHEMISTRY C

Article

pubs.acs.org/JPCC

Feasibility of Mixed Matrix Membrane Gas Separations Employing Porous Organic Cages

Jack D. Evans,[†] David M. Huang,[†] Matthew R. Hill,[†,‡] Christopher J. Sumby,[†] Aaron W. Thornton,[†,‡] and Christian J. Doonan*[,†]

[†]Centre for Advanced Nanomaterials, School of Chemistry & Physics, The University of Adelaide, Adelaide, Australia

[‡]CSIRO Materials Science and Engineering, Clayton, Australia

Supporting Information

ABSTRACT: Porous additives offer an attractive pathway to enhance the performance of polymeric gas separation membranes. Previously reported porous additives, such as zeolites and metal−organic frameworks, suffer from poor interfacial binding with the polymer matrix, which leads to nonselective gas transport pathways. Porous organic cages (POCs) are an exciting new family of soluble additives that could ameliorate these transport issues by integrating intimately with the polymer matrix. By using Voronoi network analysis, grand canonical Monte Carlo simulations, and molecular dynamics, we provide a theoretical assessment of the benefit of using POCs as additives for mixed matrix membranes (MMMs). We reveal that some MMMs containing POCs exhibit enhanced selectivity and permeability compared to the neat polymer matrix, particularly for H_2/CO_2 separations.

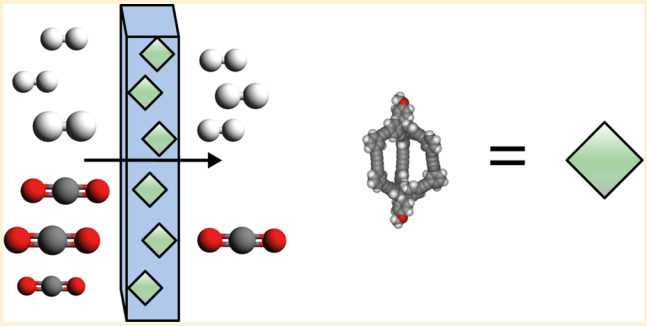

INTRODUCTION

Novel strategies that increase the efficiency of industrial gas separations are of great interest due to their direct application to green energy technologies.[1,2] The specific challenges in this area are to reduce the overall energy cost of separating (i) H_2/N_2 and H_2/CO_2 for the production of hydrogen and the precombustion capture of carbon dioxide from gasified coal following the water−gas shift reaction,[3,4] (ii) CO_2/N_2 for postcombustion "carbon capture" from gas flue streams,[5] and (iii) CO_2/CH_4 for biofuel purification and natural gas sweetening.[6]

Membrane systems are often used to perform gas separations on an industrial scale as they operate via a continuous process. This is more energy efficient than batchwise methods such as physical or chemical adsorption that require periodic energy-intensive regeneration.[3,7,8] Membranes are commonly prepared from organic polymers as they are stable, readily scalable, and cost-efficient. However, pure polymer membranes are hampered by an empirical permeability versus selectivity trade-off limit termed the "upper bound".[9,10] Accordingly, one of the current challenges in membrane separation technology is to design new materials that surpass the upper bound limit and achieve enhanced selectivity, ideally in combination with increased permeability. A promising strategy is to synthesize multi-component mixed matrix membranes (MMMs) in which a gas-selective porous solid of fixed pore diameter is embedded into a polymer host. Porous additives with narrow pore size distributions, of the order of the kinetic diameter of the target gas, can facilitate efficient size-sieving separations. Additionally, these additives can introduce chemical functionality into the polymer to improve solubility of a target gas and thus enhance membrane selectivity. Porous adsorbents that have been explored as membrane additives include zeolites, metal−organic frameworks, and zeolitic imidizolate frameworks (ZIFs).[11,13,14] Such materials have yielded MMMs that show increased permeability and selectivity compared to neat polymers.[11] However, inhomogeneity of the surface chemistry between the polymer and adsorbent can give rise to nonselective interphase voids that allow unrestricted gas diffusion.[15] This ultimately leads to less than optimal performance for these multicomponent membranes.[16] Thus, in order for MMMs to reach their full potential, synthetic methods that afford "gas-tight" integration between the two phases are required.

Recently, microporous solids composed of solution-processable porous organic cage (POC) molecules have attracted significant attention due to the potential to combine the atomic-scale control over pore size seen in MOFs and ZIFs, with the solution processability of molecular species.[17,18] These novel materials have been reported with surface areas in excess of 1500 $m^2 \cdot g^{-1}$ and have also been shown to carry out size- and shape-specific molecular separations.[19,20] It is noteworthy that for such POC materials the accessible surface area can arise from interconnection of the intrinsically porous cage cavities (intrinsic porosity), from void spaces surrounding the cages that result from inefficient packing (extrinsic porosity) or from a

Received: August 7, 2013
Revised: December 24, 2013
Published: December 30, 2013

dx.doi.org/10.1021/jp4079184 | J. Phys. Chem. C 2014, 118, 1523−1529

combination of both. As a result, polymorphs of POCs are reported to have very different physical properties.[21,22] Thus, in the present study we have used the reported crystalline structures of POCs as the basis for our feasibility analysis. This approach is validated by the work of Bushell et al. who reported MMMs incorporating a POC that showed both in situ crystal growth and crystal inclusion.[23]

Our study builds upon recent computational work that considered the use of MOFs and ZIFs as additives for MMMs. These studies have enabled the identification of important trends and targeted the development of novel materials.[24,25] POCs are attractive as they are soluble in many common organic solvents, which facilitates intimate mixing with the polymer host at the molecular scale. In silico screening will assist the development of POC-based MMMs as it can provide design principles for new materials.

Figure 1 shows the molecular structure and accessible pore surfaces of five organic cage molecules of varying cavity dimensions, pore window sizes, and molecular architectures. As the packing of cage molecules defines the bulk porosity of the materials we used the reported crystal structures of cages **1**−**5**.[17,19,21] The selectivity and permeability of MMMs containing POCs **1**−**5** were determined from grand canonical Monte Carlo (GCMC) and molecular dynamics (MD) simulations. Furthermore, we considered the effects of structural dynamics of the pore windows using Voronoi network analysis and MD simulations. To verify our modeling data, we calculated MMM permeabilities of **3** and PIM-1, a polymeric host of intrinsic microporosity, and compared these to experimental results.[23]

METHODOLOGY

To simulate the intrinsic permeabilities of **1**−**5**, we extracted their structural data from the Cambridge Structural Database.[26] Supercells (2 × 2 × 2) of structures **1**, **2**, **4**, and **5** were used and the disorder of **2** was randomly chosen across the supercell, analogous to a recent study.[27] Owing to the larger size, a single unit cell of system **3** was used and desolvated crystal structures were used where available. Structures of **1**−**5** were analyzed by Voronoi network analysis using the Zeo++ code[28,29] to calculate the accessible surface area, size, and dimensionality of the pores. A probe radius of 1.82 Å, equivalent to the kinetic diameter of N_2, was used to calculate surface areas.[30]

Equilibrium gas uptakes for H_2, N_2, CH_4, and CO_2 at 10 bar and 298 K were calculated by GCMC simulations employing the RASPA code.[31] Analogous methods have been successfully employed to model porous carbons, zeolites, and metal−organic frameworks.[25,32,33] The universal force field (UFF)[34] was used to describe the nonbonded interactions of the cage atoms. H_2 was described by the Darkrim and Levesque model,[35] N_2 and CH_4 molecules were represented using the TraPPe model,[36] and CO_2 was described using the Elementary Physics 2 model.[37] Mixed-atom interactions were expressed using Lorentz−Berthelot mixing rules.[38] The cage volume of **2** was blocked to prevent the growth of molecules in a 4 Å diameter sphere at the center of mass of the cage molecules. Inspection of the gas density plots from the simulation ensured that the cage volume was blocked and the extrinsic volume was unchanged. Each simulation used 1 million equilibration steps followed by 1 million production steps. The particular force fields chosen have precedence in literature, having been used in previous studies of MOFs.[39]

Diffusion was simulated using equilibrium MD based on the Forcite module within Materials Studio 5.0.[40] UFF was used to describe the dynamics of bonds, angles, and torsions of the

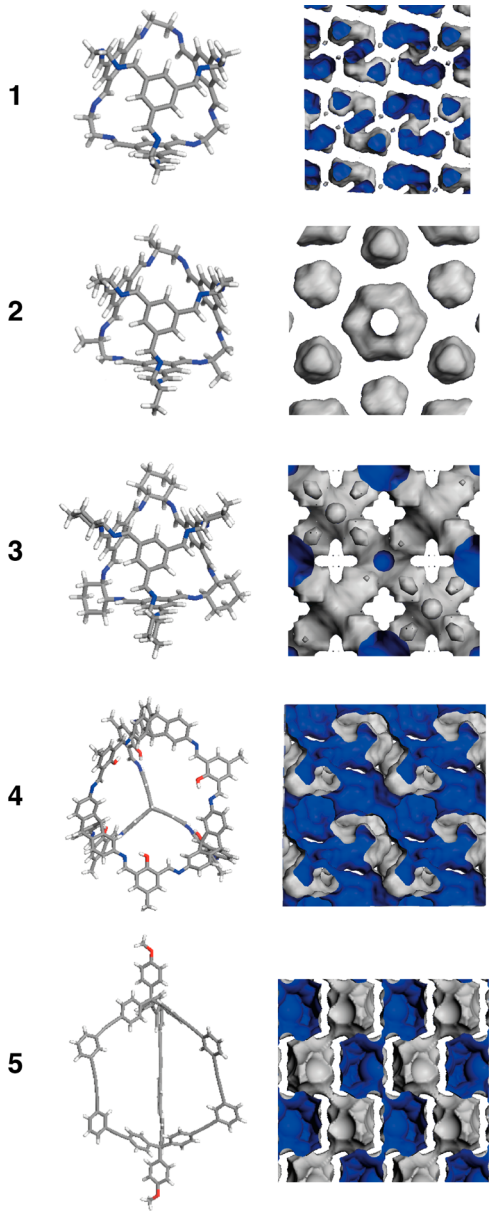

Figure 1. Summary of molecular structures and accessible pore surface (1.2 Å probe radius) of POCs **1**−**5** (gray, carbon; white, hydrogen; red, oxygen; blue, nitrogen).

systems during the MD simulation. Gas molecules at the density predicted by GCMC simulations at 10 bar were randomly placed into the crystal structure with the Amorphous Cell module. NVT dynamics were simulated for 6 ns with a time step of 1 fs with temperature controlled at 300 K using the Nosé-Hoover thermostat.[41] Only the last 5 ns of each simulation trajectory was used to calculate the mean-squared displacement of the gas molecules. The structure was allowed to be flexible to ensure that the dynamic nature of the systems was captured. A total of five unique trajectories were simulated so that an average slope of the mean-squared displacement could be calculated. The Einstein relationship in eq 1 was used to find the self-diffusivity, D_{self}, of the gas molecules from the coordinates, $\mathbf{r}(t)$, of the molecules as a function of time, t.

$$D_{self} = \frac{1}{6}\lim_{t\to\infty}\frac{d}{dt}\langle|\mathbf{r}(t) - \mathbf{r}(0)|^2\rangle \quad (1)$$

dx.doi.org/10.1021/jp4079184 | J. Phys. Chem. C 2014, 118, 1523−1529

Intrinsic permeabilities of POC crystals were approximated using eq 2, where c is the equilibrium gas concentration, and f is the operating fugacity.[42] Single-gas properties were computed and selectivity was calculated using this data.

$$P = D_{\text{self}}\frac{c}{f} \tag{2}$$

Pore dynamics were calculated using the Zeo++ code for the last nanosecond of a 2 ns NVT dynamics trajectory at 298 K in the absence of gas molecules.

MMM permeabilities were calculated for a cage volumetric fraction of 40% using the Bruggeman's effective-medium model described in eq 3, where P_{MMM} is the permeability of the MMM, P_{P} the permeability of the polymer, P_{POC} the permeability of the POC, and φ the volume fraction of POC in the membrane.[43]

$$\left(\frac{P_{\text{MMM}}}{P_{\text{P}}}\right)^{-1/3}\left[\frac{\frac{P_{\text{MMM}}}{P_{\text{P}}} - \frac{P_{\text{POC}}}{P_{\text{P}}}}{1 - \frac{P_{\text{POC}}}{P_{\text{P}}}}\right] = (1 - \varphi) \tag{3}$$

RESULTS AND DISCUSSION

Structural Properties. Figure 1 depicts POCs **1**−**5**, showing their different geometries, pore networks, and chemical functionality. Cages **1**-**3** have tetrahedral geometry of equivalent cavity size and can be differentiated by their vertex functionality. Cage **4** is an adamantoid and possesses the largest pore cavity of all the cages investigated. We note that an analogue of this structure has the highest reported surface area for a POC of 2071 $m^2 \cdot g^{-1}$.[19] Finally, cage **5** is best described as an elongated triangular dipyramid and is constructed from carbon−carbon bonds. This molecular connectivity is in contrast to cages **1**−**4**, which are composed of imine moieties.

Static pore sizes, structure metrics, and N_2-accessible surfaces areas were calculated for structures **1**−**5** (Table S-1). The internal pore cavities range from 5.4 to 9.8 Å. The pore limiting (or window) sizes for each of the crystalline POC networks were calculated to lie between 1.8 and 5.1 Å; these values are germane to size-sieving separation of industrially relevant gases N_2, CO_2, CH_4, and H_2.[44] Cages **3** and **5** possess "zeolite-type" pore structures with limiting diameters of 3.7 and 4.4 Å, respectively. Such pore architectures show excellent potential for gas separations, as they contain pore windows in the range of the kinetic diameter of target gases and also have larger cavities providing good solubility.

Structures **1**−**5** were investigated using combined GCMC and Voronoi network analysis simulations to determine representative surface areas. Good agreement between the experimental and calculated data for **1** and **2** was observed. However, discrepancies between experimental and predicted surface areas were found for the structures of cages **3**−**5**. This incongruity can be attributed to the "soft" nature of these structures, which arises from the cage molecules packing in the crystalline phase via relatively weak dispersion forces.[45] In the present study, we find that the simulated surface area of **3** is underestimated. This is anticipated as the simulation uses a "perfect" crystal and increased crystallinity of experimental samples has been shown to result in decreased surface area.[46] In addition, the dynamic pore aperture has been suggested to account for a greater N_2 porosity than expected for a static structure.[47] In contrast to structure **3**, the surface area of **4** is overestimated by a factor of 2 (2410 $m^2 \cdot g^{-1}$ compared with 1291 $m^2 \cdot g^{-1}$). This significant difference can be accounted for by a structural contraction upon solvent removal.[19] Lastly, the difference between the experimental and simulated surface area for cage **5** arises from confinement of N_2 within the pores at the experimental temperature of 77 K.[21]

Equilibrium Gas Uptake. GCMC routines are commonly used to simulate gas uptakes in porous materials. The potential parameters for the cage atoms were obtained from the UFF.

To validate our approach we simulated CO_2 and CH_4 isotherms for structures **2** and **3** and compared the results with experimental data by Tozawa et al. (Figure 2).[17] We note that

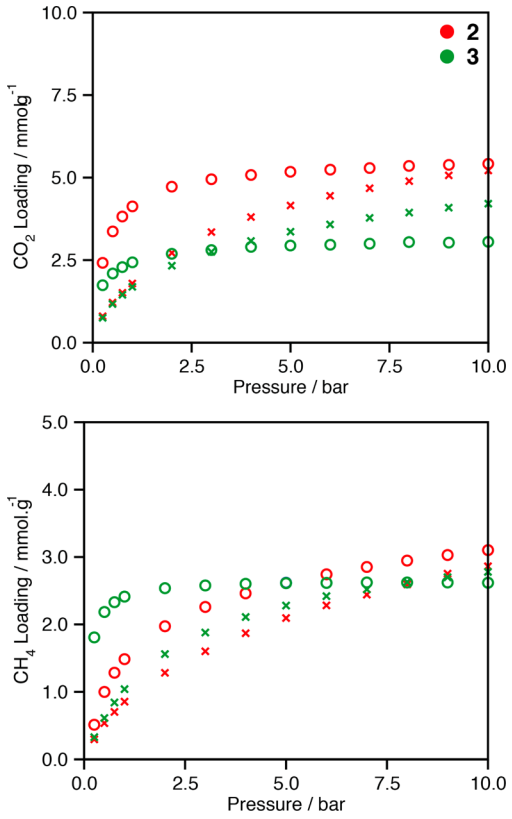

Figure 2. Comparison of experimental (crosses) and theoretical (circles) CO_2 and CH_4 isotherms of POCs **2** and **3**.

CO_2 and CH_4 gas adsorption isotherms have not been reported for **1**, **4**, and **5** and thus could not be included in this comparison. Inaccessible voids of cage **2** were blocked to ensure that the simulated isotherms were not overestimated.[48,49] Inaccessible regions observed in the static crystal structures have been found to contribute to the porosity and it is suggested that dynamic molecular motion allows diffusion into these formally inaccessible cage voids.[17,27] This process is not well understood so the amount of blocked volume was assessed to ensure the best fit to experimental data (Figure S-1). The best agreement to CO_2 and CH_4 experimental data was found for simulations containing 50 and 100% blocked cage volume, respectively.

Figure 2 shows that the larger pores of **2** result in larger uptake at high pressures for CO_2 and CH_4 adsorption. At low pressure, CH_4 has greater adsorption in **3** due to the smaller cavity sizes, which give rise to stronger binding sites from "wall−wall" potential overlaps. This effect is not observed for CO_2 adsorption because of its smaller size and aspherical shape. The observed difference between the calculated and experimental isotherms at low pressure can be attributed to artifacts in the force field, pressure-dependent accessible pockets within the structures, or

dx.doi.org/10.1021/jp4079184 | J. Phys. Chem. C 2014, 118, 1523−1529

defects in the experimental crystal. We note that in general, the gas adsorption of porous molecular crystals are inherently difficult to simulate due to their "soft" 3D structures. As such, we find the agreement to be within an acceptable range.[45] We also simulated the gas loading of H_2, N_2, CH_4, and CO_2 at 10 bar for structures **1**−**5** (Table S-2). The gas uptakes at this pressure are comparable to other porous materials such as ZIFs.[25]

Diffusion and Structural Flexibility. MD simulations at 298 K were employed to estimate the adsorbate diffusion throughout the pore structures of **1**−**5**. We selected these conditions to allow comparison with previously reported data that predicted the kinetic gas separation properties of ZIFs and MOFs.[24,25] As the series of POCs under investigation include different chemical structures a consistent generic force field (UFF) was chosen to describe all systems, in lieu of an imine-specific cage force field.[44] To assess the accuracy UFF for the imine based cages, structures **1**−**4** were optimized and compared to the crystal structures. Small discrepancies are observed between the optimized imine angles (Table S-3) and those present in the crystal structures. However, superimpositions of the optimized and crystal structure geometries of systems **1**−**5** (Figure S-2) are essentially identical, thus, demonstrating the accuracy of UFF for the range of systems compared in this study. From these MD simulations we computed the self-diffusion coefficients of **1**−**5** for H_2, N_2, CO_2, and CH_4 (Table 1).

Table 1. Self-diffusion coefficient of gas molecules in POCs[a].

	$D_{self}/10^{-10}$ m^2·s^{-1}			
cage	H_2 (2.9 Å)	N_2 (3.6 Å)	CO_2 (3.3 Å)	CH_4 (3.8 Å)
1 (1.8 Å)	0.00167	0.332	0.0161	0.00250
2 (3.9 Å)	468	11.5	5.92	3.46
3 (3.7 Å)	532	9.02	3.45	2.16
4 (5.1 Å)	762	81.7	6.43	19.4
5 (4.4 Å)	363	36.8	6.05	23.6

[a]Numbers in parentheses after the cage and gas molecule type are the pore size and gas-molecule kinetic diameter, respectively.

The diffusivities calculated are consistent with the window sizes of the structures. The diminutive pore aperture of **1** results in poor diffusion of all gas molecules. Without the specific pore size required for the kinetic separation of CO_2/N_2, the diffusivities follow the trend for the bulk diffusion of N_2 over CO_2. Structures **2** and **3** show lower diffusivity for CH_4 than CO_2, which is attributed to their limiting pore diameters of 3.9 and 3.7 Å, respectively. In contrast, the larger pore diameters of cages **4** and **5** allow the rapid diffusion of CH_4 (3.8 Å). We note that in the absence of molecular sieving, surface diffusion competes with the strong adsorption of CO_2, producing slower diffusivity of CO_2 compared with CH_4.

Our results indicate that a static pore model does not accurately represent the selectivities for CH_4 separations. As the pore structures of **1**−**5** are formed from weak intermolecular forces, it is likely that the pore window distribution is greater than that of extended frameworks in which the pore network is constructed by strong covalent bonds. Notably, pore size fluctuations have been reported to decrease the CH_4 selectivity in ZIF-8.[50] We note that the standard deviation in the window size is a reduced measure of the complicated structural dynamics and thus cannot capture all the subtleties of the dynamics of the framework structure that could potentially affect gas diffusion, such as correlated breathing motions. However, small standard deviations necessarily imply rigid windows, which likely lead to more efficient kinetic sieving. To gain further insight into the dynamic nature of the cage structures, NVT molecular dynamic simulations were carried out at analogous temperatures to the diffusion simulations described earlier. In these simulations the limiting pore size was calculated at each femtosecond over a 1 ns trajectory, after 1 ns equilibration. The resulting pore size distributions for cages **1**−**5** were calculated (see Figure 3 and Table S-4).

Based on its static structure, **2** was not expected to be a promising candidate for size sieving of CH_4, due to the crystallographic limiting pore size of 3.9 Å. However, the flexible diffusion simulations showed slower diffusivity of CH_4 than CO_2 (Table 1). We observe from the window size distributions that thermal fluctuations of **2** produce a mean window size of 3.56 Å (Table S-4), similar to that of cage **3**, thus, limiting the diffusion of CH_4.

The largest standard deviation of window sizes, 0.3 Å, was calculated for **4** (Figure 3). This may be attributed to the pore network being composed of largely extrinsic volume, which is found to fluctuate by a considerable amount over the time scale of the simulation. In contrast, the structures of **1** and **3** are found to produce narrow distributions of window sizes (standard deviations of 0.05 and 0.07 Å, respectively). The pore structures of these cages are wholly comprised of intrinsic cage volume with cage-to-cage packing linking the pore cavities. These results suggest cage molecules with functionalities that direct strong packing between molecular windows of appropriate dimensions may be more efficient for separations requiring precise size selection.

We note that the window size distribution of **3** found in the present work is different to that found in a previous study.[47] The difference can be attributed to a difference in definition: we have taken the window size to be the narrowest point in the whole cell at a given point in time, whereas the previous study assigned the window size to the diameter of the entrance to the cage cavity. Our definition, which in general gives smaller window sizes, accounts for the effects of fluctuations in the intercage regions and (mis)alignment of cage windows on the accessibility of cage volumes.

MMM Properties. Diffusion data was combined with the simulated gas uptakes to compute the permeabilities for the crystalline cage structures **1**−**5**. MMM permeabilities were extrapolated from intrinsic permeance values using Bruggeman's model, which has been shown to accurately simulate the properties of MMMs composed of polymers and ZIFs for high fractions of additives: up to 40% by volume.[51] Recent work by Bushell et al. reported the permeabilites of a MMM composed of PIM-1 and cage **3**.[23] We compared these experimental results with our simulation data to verify the use of our approach. The simulations were carried out at 1 bar to allow comparison with the experimental work. Figure 4 compares the experimental permeability of CO_2, N_2, and CH_4 with our calculated values.

Both the simulated and the experimental data show an increase in permeability for N_2, CO_2, and CH_4 with increasing loading of **3**. Although the modeled data follow the experimental trends and show good agreement with respect to N_2 permeability, the permeability of CO_2 and CH_4 is underestimated. The observed difference may suggest that additional mechanisms influence the MMM configuration, including interfacial diffusion paths produced by disruption of chain packing at the polymer−POC interface. This effect has been observed to a significant extent for

dx.doi.org/10.1021/jp4079184 | J. Phys. Chem. C 2014, 118, 1523−1529

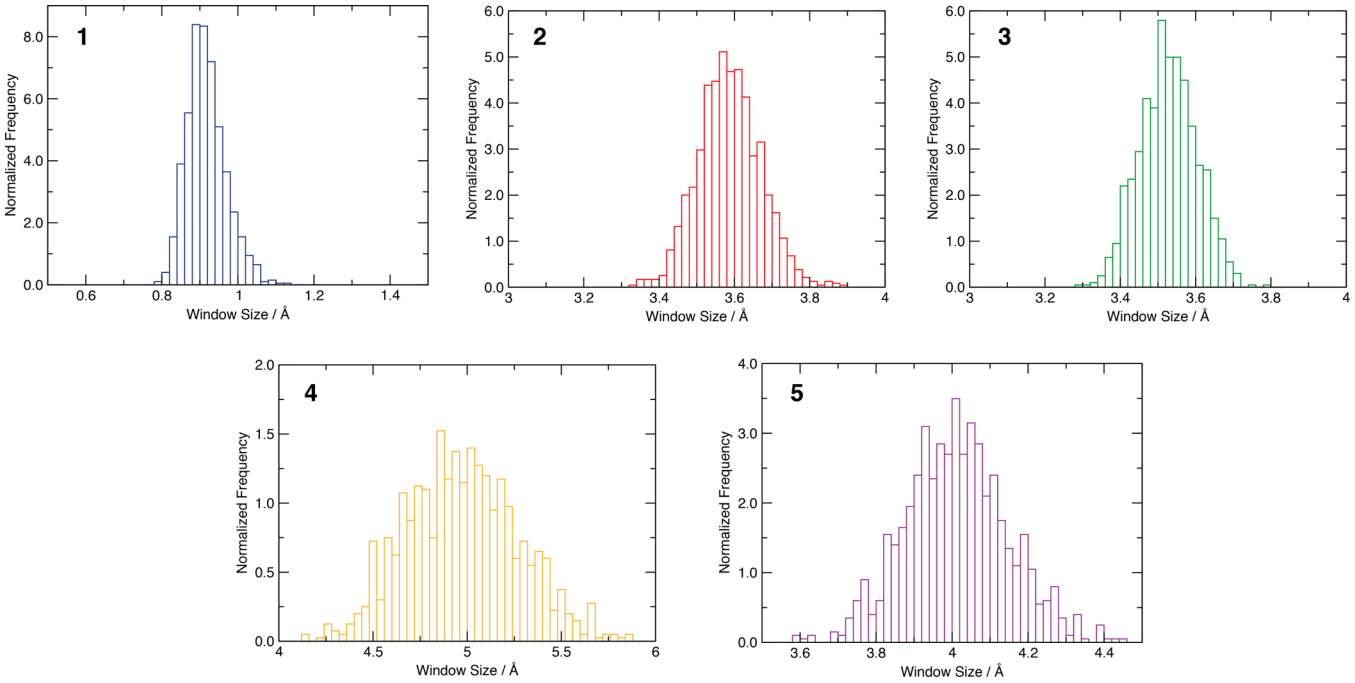

Figure 3. Window size distributions of POCs **1**−**5** over 1 ns at 298 K.

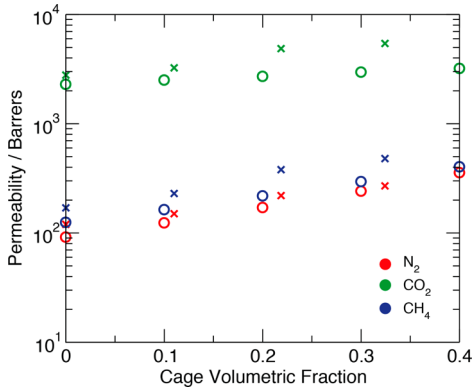

Figure 4. Comparison of the experimental (crosses) and predicted (circles) permeabilities of PIM-1:**3** at increasing loadings of **3**.

other additives in MMMs[52] and, although minimized by the organic make up of POCs, it cannot be excluded.

Using Bruggeman's model, the permeabilities and selectivities for 40% volume compositions of MMMs comprised of the polymer hosts Matrimid, Ultem, PIM-1, and PIM-7 were computed.[14,53,54] The permeability and selectivity trade-off plots for the separation of H_2/N_2, H_2/CO_2, CO_2/N_2 and CO_2/CH_4 were predicted for neat POC membranes and MMMs. These are displayed in Figure 5. We find that MMMs containing cage structures **2**−**5** significantly improve the permeability for H_2/N_2 and H_2/CO_2 separations. This enhancement is concomitant with a minor increase in the selectivity for H_2.

Figure 5 shows that the permeability for CO_2/N_2 and CO_2/CH_4 separations increases upon introduction of cages **1**−**5**, bringing the Ultem and Matrimid MMMs toward the polymer upper bound; however, a decrease in selectivity is observed for the PIM membranes. The plots for MMMs composed of cages **2**−**5** and Ultem and Matrimid show considerable overlap of data points. This is due to the difference in permeability of cages being negligible when combined with the low permeability polymer and results in MMMs with very similar permeabilities. We also note that as a result of the discontinuous pore volume of **1**, the MMMs simulated have decreased permeabilities and selectivities compared to cages **2**−**5**.

These results show that the inclusion of crystalline aggregates of POCs in neat polymer matrices result in MMMs that lie on or surpass the polymer upper bound for H_2/N_2 and H_2/CO_2 separations. The separations of CO_2 show an increase in permeability, with the addition of cage molecules advancing Matrimid-based MMMs toward the polymer upper bound. In comparison to previous studies, the performance of POC MMMs is comparable to that of predicted ZIF-containing MMMs, despite their marginally lower affinity for the investigated gases.[25] It is expected however, with the POCs' exclusively organic construction that their potential will not be hindered by poor integration between the two phases.

CONCLUSION

In summary, we have investigated a series of POC-based MMMs for the separation of industrially relevant gas mixtures H_2/N_2, H_2/CO_2, CO_2/N_2 and CO_2/CH_4. This was achieved by employing Voronoi network analysis, GCMC, and MD simulations, with the calculations compared to experimental data for validation. Conservative estimates of gas transport properties within these materials revealed that MMMs composed of POCs can exceed the polymer upper bound for H_2/N_2 separations and more substantially for H_2/CO_2 gas pair. We note the importance of considering flexibility in these materials, as weak packing forces define the pore structures. Accordingly, window size distributions over a 1 ns trajectory were calculated. These properties determined by our investigation, combined with the facile processability and good compatibility with the polymer, indicate that POC-based MMMs have exciting potential for clean energy applications.

dx.doi.org/10.1021/jp4079184 | J. Phys. Chem. C 2014, 118, 1523−1529

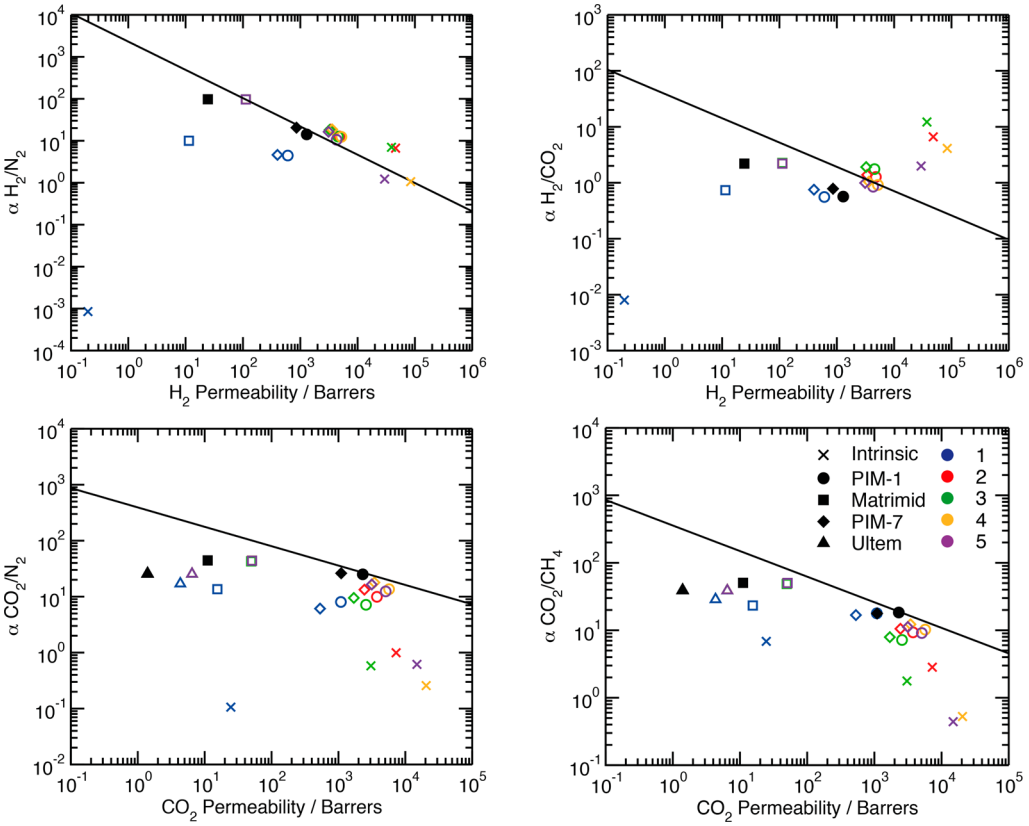

Figure 5. Permeability vs selectivity trade-off plots for neat polymers (solid black symbols), intrinsic POCs **1**−**5** (crosses), POC/polymer MMM predictions (open symbols), and Robeson's 2008 upper bound[10] (line). Open symbols represent 40% volume fraction of POC (see color code) within polymer (see symbol shape).

■ ASSOCIATED CONTENT

Supporting Information

Simulated surface areas, window sizes, cavity sizes, isotherm fitting, gas concentrations, force field validation, and distribution metrics. This material is available free of charge via the Internet at http://pubs.acs.org.

■ AUTHOR INFORMATION

Corresponding Author

*E-mail: christian.doonan@adelaide.edu.au.

Funding

Parts of this research were funded by the Science and Industry Endowment Fund (SIEF).

Notes

The authors declare no competing financial interest.

■ ACKNOWLEDGMENTS

J.D.E. thanks CSIRO Materials Science and Engineering for a Ph.D. top-up scholarship and CSIRO HPSC for computational resources. C.J.D. gratefully acknowledges the ARC for funding parts of this work (FT100100400 and DP120103909)

■ REFERENCES

(1) Haszeldine, R. S. Carbon Capture and Storage: How Green Can Black Be? *Science* **2011**, *325*, 1647−1652.

(2) Jacobson, M. Z. Review of Solutions to Global Warming, Air Pollution, and Energy Security. *Energy Environ. Sci.* **2009**, *2*, 148−173.

(3) Ku, A. Y.; Kulkarni, P.; Shisler, R.; Wei, W. Membrane Performance Requirements for Carbon Dioxide Capture using Hydrogen-selective Membranes in Integrated Gasification Combined Cycle (IGCC) Power Plants. *J. Membr. Sci.* **2011**, *367*, 233−239.

(4) Scholes, C. A.; Smith, K. H.; Kentish, S. E.; Stevens, G. W. CO_2 Capture from Pre-combustion Processes - Strategies for Membrane Gas Separation. *Int. J. Greenhouse Gas Control* **2010**, *4*, 739−755.

(5) Ho, M. T.; Allinson, G. W.; Wiley, D. E. Reducing the Cost of CO_2 Capture from Flue Gases using Membrane Technology. *Ind. Eng. Chem. Res.* **2008**, *47*, 1562−1568.

(6) Park, H. B.; Han, S. H.; Jung, C. H.; Lee, Y. M.; Hill, A. J. Thermally Rearranged (TR) Polymer Membranes for CO_2 Separation. *J. Membr. Sci.* **2010**, *359*, 11−24.

(7) Baker, R. W. *Membrane Technology and Applications*; Wiley: West Sussex, U.K., 2004.

(8) Freeman, B.; Yampolskii, Y.; Pinnau, I. *Materials Science of Membranes for Gas and Vapor Separation*; Wiley: West Sussex, U.K., 2006.

(9) Robeson, L. M. Correlation of Separation Factor versus Permeability for Polymeric Membranes. *J. Membr. Sci.* **1991**, *62*, 165−185.

(10) Robeson, L. M. The Upper Bound Revisited. *J. Membr. Sci.* **2008**, *320*, 390−400.

(11) Li, Y.; Liang, F.; Bux, H.; Yang, W.; Caro, J. Zeolitic Imidazolate Framework ZIF-7 Based Molecular Sieve Membrane for Hydrogen Separation. *J. Membr. Sci.* **2010**, *354*, 48−54.

(12) Süer, M. G.; Baç, N.; Yilmaz, L. Gas Permeation Characteristics of Polymer-Zeolite Mixed Matrix Membranes. *J. Membr. Sci.* **1994**, *91*, 77−86.

(13) Perez, E. V.; Balkus, K. J.; Ferraris, J. P.; Musselman, I. H. Mixed-Matrix Membranes Containing MOF-5 for Gas Separations. *J. Membr. Sci.* **2009**, *328*, 165−173.

(14) Ordoñez, M. J. C.; Balkus, K. J., Jr.; Ferraris, J. P.; Musselman, I. H. Molecular Sieving Realized with ZIF-8/Matrimid Mixed-Matrix Membranes. *J. Membr. Sci.* **2010**, *361*, 28−37.

(15) Mahajan, R.; Koros, W. J. Mixed Matrix Membrane Materials with Glassy Polymers. Part 1. *Polym. Eng. Sci.* **2002**, *42*, 1420−1431.
(16) Merkel, T. C.; Freeman, B. D.; Spontak, R. J.; He, Z.; Pinnau, I.; Meakin, P.; Hill, A. J. Ultrapermeable, Reverse-Selective Nanocomposite Membranes. *Science* **2002**, *296*, 519−522.
(17) Tozawa, T.; Jones, J. T. A.; Swamy, S. I.; Jiang, S.; Adams, D. J.; Shakespeare, S.; Clowes, R.; Bradshaw, D.; Hasell, T.; Chong, S. Y.; Tang, C.; Thompson, S.; Parker, J.; Trewin, A.; Basca, J.; Slawin, A. M. Z.; Steiner, A.; Cooper, A. I. Porous Organic Cages. *Nat. Mater.* **2009**, *8*, 973−978.
(18) Jiang, S.; Jones, J. T. A.; Hasell, T.; Blythe, C. E.; Adams, D. J.; Trewin, A.; Cooper, A. I. Porous Organic Molecular Solids by Dynamic Covalent Scrambling. *Nat. Commun.* **2011**, *2*, 207.
(19) Schneider, M. W.; Oppel, I. M.; Ott, H.; Lechner, L. G.; Hauswald, H. J. S.; Stoll, R.; Mastalerz, M. Periphery-Substituted [4 + 6] Salicylbisimine Cage Compounds with Exceptionally High Surface Areas: Influence of the Molecular Structure on Nitrogen Sorption Properties. *Chem.—Eur. J.* **2012**, *18*, 836−847.
(20) Mitra, T.; Jelfs, K. E.; Schmidtmann, M.; Ahmed, A.; Chong, S. Y.; Adams, D. J.; Cooper, A. I. Molecular Shape Sorting using Molecular Organic Cages. *Nat. Chem.* **2013**, *5*, 276−281.
(21) Avellaneda, A.; Valente, P.; Burgun, A.; Evans, J. D.; Markwell-Heys, A. W.; Rankine, D.; Nielsen, D. J.; Hill, M. R.; Sumby, C. J.; Doonan, C. J. Kinetically Controlled Porosity in a Robust Organic Cage Material. *Angew. Chem.* **2013**, *125*, 3834−3837.
(22) Jones, J. T. A.; Holden, D.; Mitra, T.; Hasell, T.; Adams, D. J.; Jelfs, K. E.; Trewin, A.; Willock, D. J.; Day, G. M.; Bacsa, J.; Steiner, A.; Cooper, A. I. On−Off Porosity Switching in a Molecular Organic Solid. *Angew. Chem.* **2011**, *123*, 775−779.
(23) Bushell, A. F.; Budd, P. M.; Attfield, M. P.; Jones, J. T.; Hasell, T.; Cooper, A. I.; Bernardo, P.; Bazzarelli, F.; Clarizia, G.; Jansen, J. C. Nanoporous Organic Polymer/cage Composite Membranes. *Angew. Chem., Int. Ed.* **2013**, *52*, 1253−1256.
(24) Krishna, R.; van Baten, J. M. In Silico Screening of Metal−Organic Frameworks in Separation Applications. *Phys. Chem. Chem. Phys.* **2011**, *13*, 10593−10616.
(25) Thornton, A. W.; Dubbeldam, D.; Liu, M. S.; Ladewig, B. P.; Hill, A. J.; Hill, M. R. Feasibility of Zeolitic Imidazolate Framework Membranes for Clean Energy Applications. *Energy Environ. Sci.* **2012**, *5*, 7637−7646.
(26) CSD version 5.34, Crystal Structures Database, http://ccdc.caltech.edu/, accessed July 2013.
(27) Hasell, T.; Armstrong, J. A.; Jelfs, K. E.; Tay, F. H.; Thomas, K. M.; Kazarian, S. G.; Cooper, A. I. High-Pressure Carbon Dioxide Uptake for Porous Organic Cages: Comparison of Spectroscopic and Manometric Measurement Techniques. *Chem. Commun.* **2013**, *49*, 9410−9412.
(28) Willems, T. F.; Rycroft, C. H.; Kazi, M.; Meza, J. C.; Haranczyk, M. Algorithms and Tools for High-throughput Geometry-Based Analysis of Crystalline Porous Materials. *Microporous Mesoporous Mater.* **2012**, *149*, 134−141.
(29) Martin, R. L.; Smit, B.; Haranczyk, M. Addressing Challenges of Identifying Geometrically Diverse Sets of Crystalline Porous Materials. *J. Chem. Inf. Model.* **2011**, *52*, 308−318.
(30) Jiang, S.; Jelfs, K. E.; Holden, D.; Hasell, T.; Chong, S. Y.-L.; Haranczyk, M.; Trewin, A.; Cooper, A. I. Molecular Dynamics Simulations of Gas Selectivity in Amorphous Porous Molecular Solids. *J. Am. Chem. Soc.* **2013**, *135*, 17818−17830.
(31) Dubbeldam, D.; Calero, S.; Ellis, D. E.; Snurr, R. Q. *RASPA, 1.0*, Northwestern University, Evanston, 2008.
(32) Cai, Q.; Buts, A.; Biggs, M. J.; Seaton, N. A. Evaluation of Methods for Determining the Pore Size Distribution and Pore-Network Connectivity of Porous Carbons. *Langmuir* **2007**, *23*, 8430−8440.
(33) Akten, E. D.; Siriwardane, R.; Sholl, D. S. Monte Carlo Simulation of Single- and Binary-Component Adsorption of CO_2, N_2, and H_2 in Zeolite Na-4A. *Energy Fuels* **2003**, *17*, 977−983.
(34) Rappé, A. K.; Casewit, C. J.; Colwell, K. S.; Goddard Iii, W. A.; Skiff, W. M. UFF, a Full Periodic Table Force Field for Molecular Mechanics and Molecular Dynamics Simulations. *J. Am. Chem. Soc.* **1992**, *114* (25), 10024−10035.
(35) Darkrim, F.; Levesque, D. Monte Carlo Simulations of Hydrogen Adsorption in Single-Walled Carbon Nanotubes. *J. Chem. Phys.* **1998**, *109*, 4981.
(36) Chen, B.; Siepmann, J. I. Transferable Potentials for Phase Equilibria. 3. Explicit-Hydrogen Description of Normal Alkanes. *J. Phys. Chem. B* **1999**, *103*, 5370−5379.
(37) Harris, J. G.; Yung, K. H. Carbon Dioxide's Liquid-Vapor Coexistence Curve and Critical Properties as Predicted by a Simple Molecular Model. *J. Phys. Chem.* **1995**, *99*, 12021−12024.
(38) Boda, D.; Henderson, D. The Effects of Deviations from Lorentz−Berthelot Rules on the Properties of a Simple Mixture. *Mol. Phys.* **2008**, *106*, 2367−2370.
(39) Keskin, S.; Liu, J.; Rankin, R. B.; Johnson, J. K.; Sholl, D. S. Progress, Opportunities, and Challenges for Applying Atomically Detailed Modeling to Molecular Adsorption and Transport in Metal−Organic Framework Materials. *Ind. Eng. Chem. Res.* **2008**, *48*, 2355−2371.
(40) *Materials Studio*, 5.0, Accelrys Inc., San Diego, CA, 2009.
(41) Nosé, S. A Unified Formulation of the Constant Temperature Molecular Dynamics Methods. *J. Chem. Phys.* **1984**, *81*, 511.
(42) Krishna, R.; van Baten, J. M. In Silico Screening of Zeolite Membranes for CO_2 Capture. *J. Membr. Sci.* **2010**, *360*, 323−333.
(43) Banhegyi, G. Comparison of Electrical Mixture Rules for Composites. *Colloid Polym. Sci.* **1986**, *264*, 1030−1050.
(44) Li, J. R.; Kuppler, R. J.; Zhou, H. C. Selective Gas Adsorption and Separation in Metal−Organic Frameworks. *Chem. Soc. Rev.* **2009**, *38*, 1477−1504.
(45) Li, W.; Grimme, S.; Krieg, H.; Müllmann, J.; Zhang, J. Accurate Computation of Gas Uptake in Microporous Organic Molecular Crystals. *J. Phys. Chem. C* **2012**, *116*, 8865−8871.
(46) Hasell, T.; Chong, S. Y.; Jelfs, K. E.; Adams, D. J.; Cooper, A. I. Porous Organic Cage Nanocrystals by Solution Mixing. *J. Am. Chem. Soc.* **2011**, *134*, 588−598.
(47) Holden, D.; Jelfs, K. E.; Cooper, A. I.; Trewin, A.; Willock, D. J. Bespoke Force Field for Simulating the Molecular Dynamics of Porous Organic Cages. *J. Phys. Chem. C* **2012**, *116*, 16639−16651.
(48) Krishna, R.; van Baten, J. M. Comment on Comparative Molecular Simulation Study of CO_2/N_2 and CH_4/N_2 Separation in Zeolites and Metal-Organic Frameworks. *Langmuir* **2010**, *26*, 2975−2978.
(49) Kim, J.; Martin, R. L.; Rübel, O.; Haranczyk, M.; Smit, B. High-Throughput Characterization of Porous Materials Using Graphics Processing Units. *J. Chem. Theory Comput.* **2012**, *8*, 1684−1693.
(50) Haldoupis, E.; Watanabe, T.; Nair, S.; Sholl, D. S. Quantifying Large Effects of Framework Flexibility on Diffusion in MOFs: CH_4 and CO_2 in ZIF-8. *ChemPhysChem* **2012**, *13*, 3449−3452.
(51) Keskin, S.; Sholl, D. S. Selecting Metal Organic Frameworks as Enabling Materials in Mixed Matrix Membranes for High Efficiency Natural Gas Purification. *Energy Environ. Sci.* **2010**, *3*, 343−351.
(52) Shimekit, B.; Mukhtar, H.; Murugesan, T. Prediction of the Relative Permeability of Gases in Mixed Matrix Membranes. *J. Membr. Sci.* **2011**, *373*, 152−159.
(53) Vu, D. Q.; Koros, W. J.; Miller, S. J. Mixed Matrix Membranes using Carbon Molecular Sieves: I. Preparation and Experimental Results. *J. Membr. Sci.* **2003**, *211* (2), 311−334.
(54) Budd, P. M.; Msayib, K. J.; Tattershall, C. E.; Ghanem, B. S.; Reynolds, K. J.; McKeown, N. B.; Fritsch, D. Gas Separation Membranes from Polymers of Intrinsic Microporosity. *J. Membr. Sci.* **2005**, *251*, 263−269.